THE JOURNAL OF PHYSICAL CHEMISTRY C

Article

pubs.acs.org/JPCC

Modeling the Aggregation of MgO Clusters on Highly Oriented Graphite

F. Calvo,*[,†] K. Bowen,[‡] and X. Tang[‡]

[†]ILM, CNRS UMR 5306 and University of Lyon, 43 Bd du 11 Novembre 1918, F69622 Villeurbanne Cedex, France

[‡]Department of Chemistry, Johns Hopkins University, Baltimore, Maryland 21218, United States

ABSTRACT: Nanoscale assemblies hold great potential for the design of novel materials with tunable properties. The main factors driving the assembly are the interactions between the building blocks together or with their environment, as well as their intrinsic properties, starting with their size. In the present work, we have modeled the aggregation between magnesium oxide clusters $(MgO)_n$ soft-landed on highly oriented pyrolytic graphite (HOPG), including atomistic details. Our approach includes a many-body polarizable potential for magnesium and oxide ions that takes into account the polarizability and the corrugation of the graphite substrate, and a simplified version of this potential for simulating larger self-assemblies. The simulations show that $(MgO)_n$ clusters aggregate into fractal-like islands in the case of the magic size $n = 32$, coalescence being driven by rotation and reorientation of individual cubic clusters. Rocksalt order is locally preserved, although oriented aggregation is hindered by the presence of voids due to geometric frustration in the ramified arrangement. In contrast, the self-assembly of $(MgO)_{13}$ clusters is much more globular, as a result of a broader variety of conformers exposing very different faces to one another. Our predictions highlight the importance of geometry on substrate-mediated cluster interactions, and are supported by experiments on chemically and structurally analogous PbS clusters.

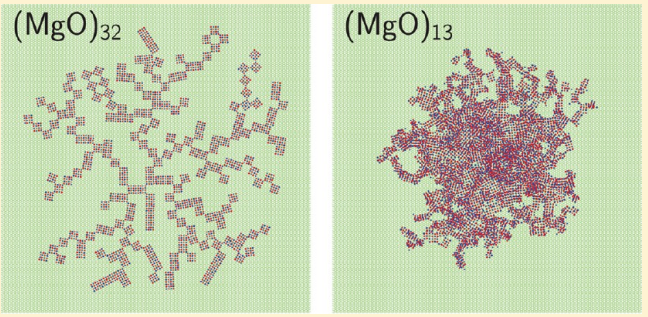

1. INTRODUCTION

The assembly of nanoscale particles can be used to create bidimensional or tridimensional superlattices[1−3] or to grow anisotropic structures such as nanowires or nanosheets by so-called oriented aggregation.[4−8] Both types of materials are promising for a broad range of applications, with the main motivation being to exploit the tailored properties of individual clusters playing the role of superatoms, and upscale those properties to more macroscopic dimensions through the arrays those building blocks can form. The main challenges lie in the synthesis of those clusters and the possible need for monodisperse samples, and the control of the assembly through the precise characterization of the cluster−cluster interaction. The rules that govern the assembly also involve the environment. Arrays obtained from colloidal chemistry require the removal of the solvent, which should not interact too strongly with the particles. In the case of bidimensional supracrystals, the particles are deposited on a substrate, which may hinder or promote self-assembly. Tailoring the environment with the substrate may thus be equally as important as the building blocks themselves, as illustrated by the recent suggestion to use graphene[9] or boron nitride[10] as nanomesh templates for driving bidimensional arrays.

Relatively large inorganic nanoparticles with diameters approaching 10 nm have been successfully used as building blocks for self-assembled materials.[11,12] The colloidal synthesis of those particles allows for a large diversity in their shape and interactions, providing some further way to direct assembly or growth.[13−15] Alternatively, assemblies can be produced from the soft deposition of individual particles that are preformed in the gas phase.[1,16−18] The technique is valuable because the clusters can be properly size-selected, their properties being preserved during soft landing. However, the resulting assembly depends on a number of energetic and especially kinetic factors,[19] which makes it generally difficult to predict quantitatively the type of assembly obtained from a known building block, beyond purely phenomenological approaches that neglect microscopic details.[19−23]

Owing to mass spectrometry techniques, clusters prepared in the gas phase for subsequent assembly are highly monodisperse. In this regime, where each atom counts, "magic" clusters having a particularly stable size or composition are also better candidates for applications, because this higher stability is expected to convey to the assembled material.[24] However, this superior stability before and after assembly may not be necessarily preserved during the assembly process, and it is important that the clusters are robust against deformation, coalescence, and sintering.[25]

In contrast to ligand-protected colloidal nanoparticles, the interaction between very small clusters can hardly be described

Received: October 16, 2013
Revised: December 12, 2013
Published: December 16, 2013

   dx.doi.org/10.1021/jp410259b | J. Phys. Chem. C 2014, 118, 1306−1317

by empirical models as it requires some careful attention to the details of geometric structure.[3] Quantum chemistry methods such as density-functional theory, although suitable for electronic and optical properties, are not practical for simulating large assemblies containing multiple clusters formed over nanoseconds or more. In the present work, we show how dedicated computational methods based on accurate potential energy surfaces can be used to model the assembly process at the atomistic level and shed light onto the dependence of the resulting assembly on the building block, the importance of the cluster−substrate interaction, and the time scales needed for possible oriented aggregation.

Magnesium oxide clusters deposited on highly oriented pyrolytic graphite (HOPG) have been chosen as a realistic system for this investigation, owing to the substantial amount of work already devoted to those clusters from experimentalists[26,27] and theoreticians.[27−36] Being dominantly ionic, chemical bonding in MgO clusters leads to stable structures with cubic or hexagonal motifs.[27] Stoichiometric clusters are furthermore insulating, hence bind only weakly to the graphite substrate. Another motivation of the present work lies in the analogy between MgO and PbS clusters, which also form 'baby crystals' at the specific size of 32 pairs of ions.[37] The assembly of PbS nanoclusters on graphite was shown to be dominated by orientated aggregation at low coverage,[37] emphasizing the role played by this mechanism in the low-density limit. In absence of accurate model potentials for PbS, MgO clusters on HOPG thus appear as good candidates to evaluate the combined influences of the cluster−cluster and cluster-substrate interactions on the resulting self-assembly, especially in the high-density case where clusters are deposited over short time scales. As shown by our simulations, the size of the clusters plays an important role through the stable structure(s) it imposes on the deposited clusters.

The modeling strategy followed here consists first of building an accurate potential energy surface (PES) for $(MgO)_n$ clusters deposited on graphite. A coarse-grained approached was used, in which the substrate is treated implicitly in order to alleviate most of the computational cost, also enabling simulations of large assemblies on a statistical footing. The PES is used to locate the stable configurations of individual clusters and their dimers as key intermediates in the formation of larger assemblies. For this purpose, a combination of optimization methods and all-atom molecular dynamics (MD) simulations were carried out. Due to its many-body character, the potential is too computationally intensive for simulating thousands of atoms, and we have used a simpler approximation where the assembly is grown sequentially by addition of rigid building blocks followed by a local relaxation on the complete PES. The model predicts sensitively different assemblies depending on the building monomer, and highlights the crucial role of structure already on the formation of stable intermediate dimers. Experimental data on the assembly of $(PbS)_{32}$ clusters at high coverage supports our findings of a dendritic pattern.

The article is organized as follows. In the next section, we further detail the computational strategy used to model self-assembly of MgO clusters on HOPG at the level of atomistic details, and the potential energy surface developed for those systems. The results are presented and discussed in sections 3 and 4 for the dimers and the larger assemblies, respectively, before some concluding remarks are drawn in section 5.

2. METHODS

Our modeling of the self-assembly of MgO clusters on graphite ultimately relies on the direct simulation, by molecular dynamics, of the successive coalescence of individual building blocks onto a seed. To better understand the assembly mechanisms, we have focused first on the interaction between two individual clusters, and on the underlying role of geometry on the products obtained upon such soft collisions. Throughout this computational work, we will be employing atomistic potential energy surfaces describing the MgO clusters interacting on the perfect graphite substrate. A simple but accurate polarizable model was developed here, combining an existing potential for bare magnesium oxide clusters with a chemically realistic contribution from the substrate, treated at a coarse-grained level but, for consistency, also accounting for polarization effects.

2.1. Polarizable Potential for Isolated $(MgO)_n$ Clusters.

We start from the polarizable fluctuating-charges potential previously developed for isolated MgO clusters,[32] that we briefly recall here. In this model, the partially covalent-ionic bonding arises from the balance between some short-range Pauli repulsion and a long-range electrostatic attraction, with some important contribution of charge transfer due to the electronegativity difference between the magnesium and oxygen ions. The use of fluctuating charges allows to represent the dependence of the charge of an ion on its environment, in particular its coordination. In addition, the model accounts for the significant deformation of the chemical bonds caused by explicit polarization forces.

We denote by $\mathbf{r}_i$ and q_i the position and charge carried by ion i. The potential energy $V(\mathbf{R})$ of the configuration $\mathbf{R} = \{\mathbf{r}_i\}$ made of N ions consists of two main contributions, $V = V_{rep} + V_Q$ in which V_{rep} is a pairwise Pauli repulsion and V_Q the electrostatic and polarization contribution. Following ref 32, V_{rep} is taken as a Born−Mayer form,

$$V_{rep}(\mathbf{R}) = \sum_{i<j} D \exp(-\beta r_{ij}) \tag{1}$$

where D and β are two parameters. The electrostatic contribution is expressed within a fluctuating-charges framework[38,39] as

$$V_Q(\mathbf{R}) = \sum_i \left[\nu_i q_i + \frac{1}{2}U_{ii}^0 {q_i}^2 - \frac{1}{2}\alpha {\mathbf{E}_i}^2\right] + \sum_{i<j} J_{ij}(r_{ij}) q_i q_j + \lambda\left(Q - \sum_i q_i\right) \tag{2}$$

In the above equation, ν_i refers to the electronegativity of element i, U_{ii}^0 to its hardness, and α_i to its isotropic atomic polarizability. J_{ij} is the Coulomb integral between ions i and j, modeled according to the Ohno representation[40] as

$$J_{ij}(r) = \frac{1}{[r^2 + (U_{ii}^0)^{-2} \exp(-\gamma_{ij} r^2)]^{1/2}} \tag{3}$$

in such a way that $J_{ii}(r)$ tends to U_{ii}^0 as r goes to 0. The electric field vector $\mathbf{E}_i$ at the site of ion i reads

$$\mathbf{E}_i = \sum_{j\neq i} -q_j \frac{\partial J_{ij}}{\partial \mathbf{r}_i} \tag{4}$$

At a fixed geometry $\mathbf{R}$, the charges $\{q_i\}$ are determined so as to minimize the overall electrostatic energy under the constraint

dx.doi.org/10.1021/jp410259b | J. Phys. Chem. C 2014, 118, 1306−1317

of charge conservation, as expressed by the last term of eq 2 with the Lagrange multiplier λ. Owing to the linear dependence of the electric field on the charges, the electrostatic energy is quadratic and can be minimized exactly, using, for example, linear algebra. In practice, those charges are obtained as solution of the matrix equation $\mathbf{CX} = \mathbf{D}$, where $\mathbf{X} = \{q_i,\lambda\}$ is a $N + 1$ vector, $\mathbf{D}$ has components $D_i = -\nu_i$ for $i \leq N$ and $D_{N+1} = Q$, and the element C_{ij} of the matrix $\mathbf{C}$ is

$$C_{ij} = J_{ij} - \sum_k \alpha_k \left(\frac{\partial J_{ki}}{\partial \mathbf{r}_k} \frac{\partial J_{kj}}{\partial \mathbf{r}_k} \right) \tag{5}$$

The parameters of the model were initially optimized in order to reproduce the properties of the MgO dimer, in which the charge transferred is approximately 1, and the MgO rocksalt crystal, where the charge transferred is increased to about 2 due to the absence of residual electrostatic field. In the present work, they were slightly adjusted again in order to reproduce the greater stability of $(MgO)_{3n}$ hexagonal nanotubes recently evidenced by a combined experimental/theoretical investigation.[27] Those updated parameters are listed in Table 1.

Table 1. Parameters of the Polarizable Fluctuating-Charges Potential for Isolated MgO Clusters, Updated from Ref 32 to Improve the Relative Stability of Hexagonal Nanotube Clusters

parameter	Mg	O	Mg−O
D (eV)	6274	6274	6274
β (Å^{-1})	4.90	4.90	4.90
U_{ii}^0 (eV)	12.5	30.7	8.1
γ (Å^{-2})	0.53	0.54	0.33
ν (eV)	23.5	0	
α (Å^3)	0.17	3.36	

2.2. Repulsion−Dispersion Interaction with the HOPG Substrate. The interaction between the MgO clusters and the HOPG substrate is dominated by weak dispersion forces that can be reasonably represented by a Lennard−Jones (LJ) potential. The resulting potential V_{HOPG} between the MgO cluster and the graphite substrate is then formally expressed as

$$V_{HOPG} = \sum_{i\in MgO} V_{HOPG}^{(i)} = \sum_{i\in MgO} \sum_{j\in HOPG} 4\varepsilon_{ij} \left[\left(\frac{\sigma_{ij}}{r_{ij}} \right)^{12} - \left(\frac{\sigma_{ij}}{r_{ij}} \right)^{6} \right] \tag{6}$$

where ε_{ij} and σ_{ij} are the energy and distance parameters of the LJ interaction between ion i and carbon atom j. Appropriate values for those parameters were taken from the OPLS force field.[41]

Close to room temperature, the substrate is not expected to undergo strong vibrational motion, and can be taken as rigid in good approximation. This assumption is mostly for computational convenience, but it precludes vibrational redistribution at the cluster−substrate contact, a feature that will be mimicked in a more empirical manner (see below). We have followed a standard strategy in surface physics[42] consisting of using an analytical approximation for the sum over carbon atoms in the previous equation. Assuming that the substrate is perpendicular to the z axis, we thus replace the infinite sum of LJ interactions by the Fourier series truncated here at the second harmonics:[42]

$$V_{HOPG}^{(i)} = V_0^{(i)}(z_i) + V_1^{(i)}(z_i) f_1(x_i, y_i) + V_2^{(i)}(z_i) f_2(x_i, y_i) \tag{7}$$

in which f_1 and f_2 have the periodicity associated with (0001) graphite. In Cartesian coordinates, those corrugation functions read

$$f_1 = -2\left[\cos\frac{2\pi}{a\sqrt{3}}\left(x_i - \frac{y_i}{\sqrt{3}} \right) + \cos\frac{2\pi}{a\sqrt{3}}\left(x_i + \frac{y_i}{\sqrt{3}} \right) + \cos\frac{4\pi}{3a} y_i \right]$$

$$f_2 = +4\left[\cos\frac{2\pi}{a\sqrt{3}}(x_i - y_i\sqrt{3}) + \cos\frac{2\pi}{a\sqrt{3}}(x_i + y_i\sqrt{3}) + \cos\frac{4\pi}{a\sqrt{3}} x_i \right] \tag{8}$$

where a = 1.42 Å is the lattice parameter of graphite. The successive contributions $V_k^{(i)}$ to the Fourier expansion were initially taken from Steele, and the recommended form was chosen for V_0 as[42]

$$V_0^{(i)}(z_i) = W_0^{(i)} \left[\frac{2A_6^{(i)}}{5\tilde{z}_i^{10}} - \frac{1}{\tilde{z}_i^4} - \frac{1}{3\Delta z(\tilde{z}_i + 0.61\Delta z)^3} \right] \tag{9}$$

where $\tilde{z}_i = z_i/\sigma_{iC}$, $A_6^{(i)} = (\sigma_{iC}/a\sqrt{3})^6$, Δz = 1.38, and $W_0^{(i)} = 8\pi A_6^{(i)}/\sqrt{3}$.

The expressions for $V_1^{(i)}$ and $V_2^{(i)}$ involve the Bessel functions of the second kind K_2 and K_5,[42] and for the graphite substrate they read[42]

$$V_1^{(i)}(z_i) = \frac{1}{2} W_0^{(i)} \left[\frac{A_6^{(i)}}{30} \left(\frac{2\pi}{\tilde{z}_i\sqrt{3}} \right)^5 K_5(4\pi\tilde{z}_i/\sqrt{3}) - 2\left(\frac{2\pi}{\tilde{z}_i\sqrt{3}} \right)^2 K_2(4\pi\tilde{z}_i/\sqrt{3}) \right]$$

$$V_2^{(i)}(z_i) = \frac{1}{2} W_0^{(i)} \left[\frac{A_6^{(i)}}{30} \left(\frac{2\pi}{\tilde{z}_i} \right)^5 K_5(4\pi\tilde{z}_i) - 2\left(\frac{2\pi}{\tilde{z}_i} \right)^2 K_2(4\pi\tilde{z}_i) \right] \tag{10}$$

The above functions were calculated numerically in a broad range of distances, and accurate approximations were found as

$$V_k^{(i)}(z_i) \simeq \chi_k \frac{\exp(-b_k z_i)}{z_i^{a_k}} \tag{11}$$

in which the dependence of the parameters χ_k, b_k, and a_k on the ion type i was omitted for clarity. The various parameters for the repulsion−dispersion interactions between the magnesium or oxygen ions and the HOPG substrate are given in Table 2, including the LJ parameters σ and ε from which the numerical approximations for V_1 and V_2 are extracted.

2.3. Contribution of the Substrate to the Polarization Energy. The graphite substrate is an anisotropic polarizable medium, and upon contact of ions some image charges are created, leading to an additional contribution to the binding energy. This leads to a new term in the fluctuating charges model, involving the response of the electric field due to the

dx.doi.org/10.1021/jp410259b | J. Phys. Chem. C 2014, 118, 1306−1317

Table 2. Parameters of the Repulsion−Dispersion Interaction between Magnesium or Oxygen Ions and the Graphite Substrate

parameter	Mg	O
ε (meV)	107.3	45.14
σ (Å)	2.597	3.335
χ_1 (10^6 au)	1.179	3.190
b_1 (Å^{-1})	3.454	2.966
a_1	0.139	0.137
χ_2 (10^6 au)	2.436	10.033
b_2 (Å^{-1})	4.307	3.935
a_2	0.344	0.364

ions parallel and perpendicular to the graphite surface. Following González and co-workers,[43] the polarization energy due to the MgO ions on the graphite substrate is written as $V_{pol}(\mathbf{R}) = V_{\parallel}(\mathbf{R}) + V_{\perp}(\mathbf{R})$ with

$$V_{\parallel}(\mathbf{R}) = -\sum_i \left[\frac{q_i^2}{4z_i} - \frac{1}{2}\sum_{j\neq i} \frac{q_i q_j}{r'_{ij}} \right]$$

$$V_{\perp}(\mathbf{R}) = -\sum_i \left[\frac{2\pi\alpha_{\perp} q_i^2}{8z_i^2} - \frac{1}{2}\sum_{j\neq i} \frac{2\pi\alpha_{\perp} q_i q_j (z_i + z_j)}{(r'_{ij})^3} \right] \quad (12)$$

with $\alpha_{\perp} \approx 0.220$ Å being the polarizability density of the graphite surface.[43] In the above equations, r'_{ij} is the distance between charge q_i at the site $\mathbf{r}_i$ of ion i and the mirror image $(x_j, y_j, -z_j)$ of ion q_j located at $\mathbf{r}_j(x_j, y_j, z_j)$.

In the framework of the fluctuating charges model, the charges must be solved self-consistently with this extra contribution, and this leads to a new matrix $\mathbf{C}$ with elements such that

$$C_{ii} \rightarrow C_{ii} - \frac{1}{4z_i} - \frac{2\pi\alpha_{\perp}}{8z_i^2}$$

$$C_{ij} \rightarrow C_{ij} - \frac{1}{r'_{ij}} - \frac{2\pi\alpha_{\perp}(z_i + z_j)}{(r'_{ij})^3} \quad (13)$$

2.4. Computational Details. Two clusters were selected to illustrate the role of size and structure on the aggregation process, namely, $(MgO)_{32}$ and $(MgO)_{13}$. While the former is particularly stable as a 4 × 4 × 4 piece of rocksalt crystal, the latter has a number of isomers close in energy, whose relative stability is further affected by deposition on HOPG. Upon coalescence, the two clusters can form various products, from which the larger self-assembly highly depends. It is thus important to characterize the dimers produced along those early steps of coalescence. Molecular dynamics simulations of collisions under mild conditions (300 K kinetic energy) were carried out by randomly selecting the orientations and, in the case of $(MgO)_{13}$, the isomers of the two clusters. The impact parameter b of the collision was also randomly selected assuming uniformly distributed collisions, according to the probability $p(b)\,db \propto 2\pi b\,db$ within a range $0 \leq b \leq b_{max} = 10$ Å. Statistics were accumulated over reactive collisions only, from a pool of 10^4 independent trajectories.

The self-assembly of multiple clusters was simulated by assuming a successive growth by individual monomers. From experiments on soft-landing ions on HOPG,[44] we can reasonably assume that the incident ionized clusters soft-landed on HOPG would neutralize upon contact with the uppermost graphene layers due to its conductivity. The clusters in the multiple assembly process are thus considered as neutral. A two-stage approach was followed to model the assembly process, in which a new cluster is thrown at the existing assembly with 300 K kinetic energy, both target and projectile being treated as rigid bodies and with fixed charges taken from the solution of the initial fluctuating charges model. These two approximations were found necessary in order to enable simulations of hundreds of monomer clusters, individual clusters being added one at a time over tens of picoseconds. Here a description by quaternions was employed to propagate the equations of motion. In this stage, the impact parameter and initial orientation of the cluster were both taken at random.

With this procedure, the projectile is guaranteed to connect with the existing assembly. Once the distance between the two coalescing compounds came below a threshold of 5 Å, the MD simulation was smoothly stopped by introducing a friction force, in such a way that the velocity of the incoming cluster were reduced by 0.01% every time step. This cooling process was used to mimic the dissipation of translational kinetic energy brought by the collision onto the vibrational modes of both the targetted assembly and the HOPG substrate, which are altogether neglected in the present simplified coarse-grained approach. Next, a local relaxation of all atomic degrees of freedom of the entire assembly (including the last added cluster) was performed, still keeping fixed all partial atomic charges. By repeating this procedure several hundreds times, assemblies containing more than 10^4 atoms could be produced and analyzed.

The MD trajectories of cluster−cluster coalescence employed a time step of 1 fs and were propagated over 100 ps each. The initial configurations in phase space, before addition of 300 K relative translational energy, were sampled in the canonical ensemble at 300 K as generated by the Nosé-Hoover method. The MD trajectories of assembly growth with rigid building blocks used a longer time step of 2 fs.

3. EARLY STAGES OF ASSEMBLY: FROM MONOMER TO DIMER

Under appropriate conditions, the interactions between mesoscopic particles can be described based on effective theories such as the one due to Hamaker.[45] However, at the nanoscale, the geometric details due to facetting become important, as well as the dynamical reorientation during attachment.[6,46,47] In the present case of ionic compounds, the interactions between atoms are furthermore highly heterogeneous and the orientation of the two interacting clusters significantly impacts the coalescence product.[6] In order to assess the role of the substrate on the dimers formed by spontaneous coalescence, we have simulated collisions between two $(MgO)_{32}$ building blocks either in the gas phase or between deposited clusters. The possible presence of the substrate affects the simulations through the rotational degrees of freedom of the initially colliding systems: While clusters in the gas phase are allowed to rotate freely around their center of mass (3D rotation), deposited clusters always expose a face parallel to the graphite surface (axial rotation) in order to maximize the surface interaction energy. This constraint significantly reduces the number of possible coalescence products obtained in the simulations, as illustrated in Figure 1. Those products can be labeled as $n \times p$ according to the

dx.doi.org/10.1021/jp410259b | J. Phys. Chem. C 2014, 118, 1306−1317

number of ions in contact, and their binding energies are given in Table 3 together with the lowest vibrational frequency.

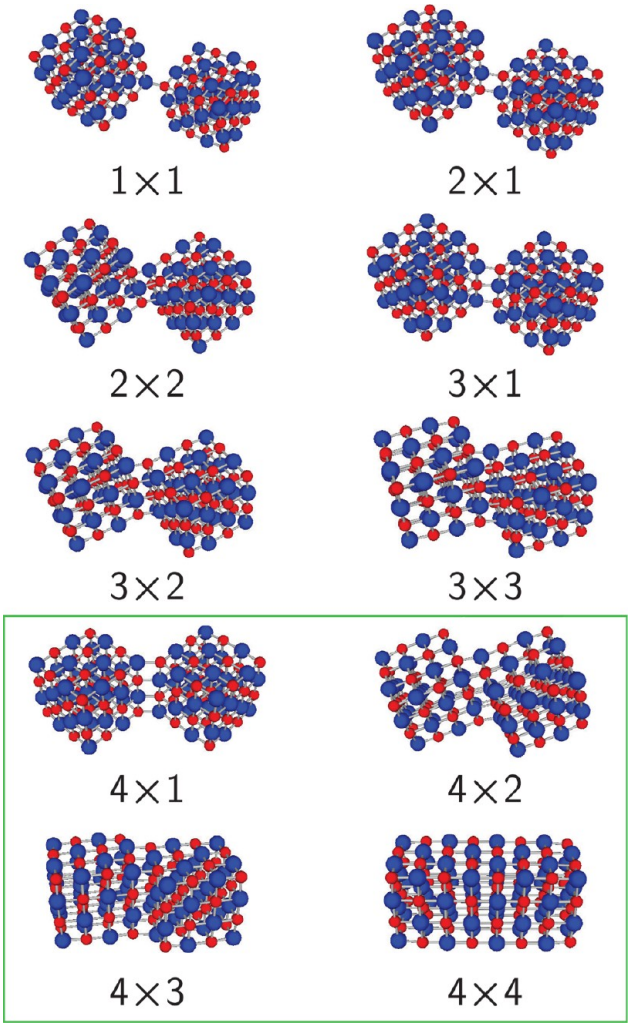

Figure 1. Dimers $n \times p$ produced by coalescence of two $(MgO)_{32}$ cluster units, in which n and p designate the number of ions in contact. The $1 \times 1^*$ product, which connects the two monomers only by a single bond, is not a local minimum. Only products with $n = 4$ can be formed on the HOPG substrate, as indicated in the green frame.

Collisions in the gas phase can produce dimers of $(MgO)_{32}$ clusters connected along vertices only (1×1) or edges $(n \times 1, n > 1)$. Except for the 1×1 dimer, all those structures are locally stable, with very soft vibrational modes involving the global relative motion of the two monomeric clusters around the bonds connecting them. The 4×1 dimer is the only product of this type that can be obtained on the HOPG substrate, other $n \times p$ dimers with $n < 4$ being unable to accommodate contact with the substrate without significant deformation. More strongly bound dimers with $p > 1$ can also be produced if the two initial clusters share more than a string of ions in contact. Again, coalescence on the graphite substrate entails $p = 4$ with n ranging from 2 to 4 depending on the common area between the two clusters, whereas collisions in the gas phase do not impose any such limitation.

The softest vibrational modes reported in Table 3 are also insightful about the relative interaction strengths: the single $(MgO)_{32}$ cluster has its lowest-frequency mode near 100 cm^{-1}

Table 3. Energetic and Vibrational Properties of $(MgO)_{32}$ Dimer Products, Labeled as $n \times p$ Where n and p Designate the Number of Ions in Contact[a]

	isolated		deposited	
system	energy	ω_{min} (cm^{-1})	energy	ω_{min} (cm^{-1})
monomer	7.24 eV/ion	101	7.27 eV/ion	20
dimer				
1×1	+1.01 eV	$2i$		
2×1	+1.73 eV	3		
2×2	+1.99 eV	9		
3×1	+2.01 eV	4		
3×2	+3.16 eV	19		
4×1	+2.93 eV	4	+2.90 eV	4
4×2	+3.97 eV	22	+3.93 eV	20
4×3	+5.71 eV	40	+5.70 eV	23
4×4	+8.27 eV	51	+8.21 eV	23

[a]The absolute binding energies are given in eV/ion for the monomer, and adsorption energies relative to two individual monomers are given for the dimers. Note that the 1×1 product is metastable with an imaginary lowest frequency.

in the gas phase, but only 20 wavenumbers after deposition on graphite. The corresponding normal mode relates to some vertical oscillation of the entire cluster on the substrate, which due to the relative weakness of this interaction happens to be significantly lower than 100 cm^{-1}. The lowest frequency modes of the dimers of $(MgO)_{32}$ do not exceed 51 cm^{-1}, and increase with the number of intercluster bonds (both n and p increasing). In particular, the 4×1 dimer has a low but positive mode at only 4 cm^{-1} which corresponds to the overall oscillation of the two cubes around their edge-sharing axis. This mode is preserved in the deposited dimer, although in other $4 \times p$ products the cluster-substrate interaction is again responsible for the softest mode near 20 cm^{-1}.

The statistics of dimers produced by coalescence can be discussed on a more quantitative basis, the probabilities of forming all possible $n \times p$ products from collisions between $(MgO)_{32}$ monomers at 300 K kinetic energy being represented as histograms in Figure 2. Collisions resulting in the scattering of the two clusters amount to about 4–9% under the present choice of maximum impact parameter $b_{max} = 10$ Å and at 300 K translational energy. Among all possible $n \times p$ products, only those bound along an edge $(n \times 1)$ or collapsing face to face $(4 \times p)$ are found in significant amounts. However, only the latter have really large proportions, in agreement with their much greater energetic stability given in Figure 1.

The substrate has a major influence on the dimers produced by such mild collisions, the initial clusters already sharing a parallel face (this notably explains the absence of $n \times p$ products with $n < 4$). The chances of forming a dimer are thus higher by 5%, and the more stable $4 \times p$ products with $p > 1$ are also more likely by 20% with respect to gas-phase conditions. In particular, the 4×2 and 4×3 products are now obtained more often due to favorable exposures of ions of opposite sign during the final approach between the monomers.

The less stable $n \times 1$ dimers are surprisingly present among the products, both in the gas phase and on the HOPG substrate. In particular, the edge-bonded 4×1 dimer is highly probable after 100 ps. Although those products are energetically not the most stable, their low vibrational modes contribute to increasing their entropy and enhancing their finite temperature

dx.doi.org/10.1021/jp410259b | J. Phys. Chem. C 2014, 118, 1306–1317

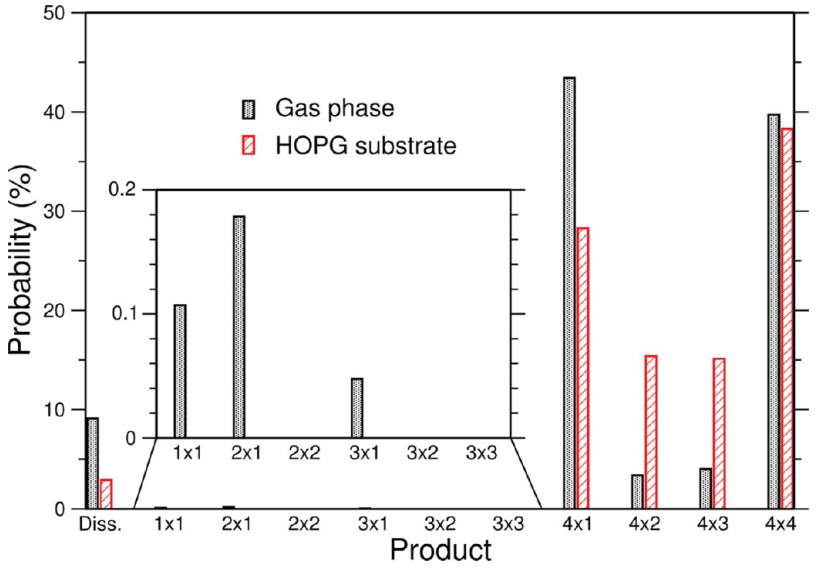

Figure 2. Probability distribution of forming a specific product upon coalescence of two $(MgO)_{32}$ cluster units, in the gas phase and on the HOPG substrate.

stability. But their formation immediately after contact indicates that the potential energy surface is funneled toward those conformations, which are thus further favored by the collisions kinetics. Inspection of the MD trajectories reveals that 4 × 4 products can actually be obtained after a transient period spent in the 4 × 1 dimer. This is illustrated in the inset of Figure 3,

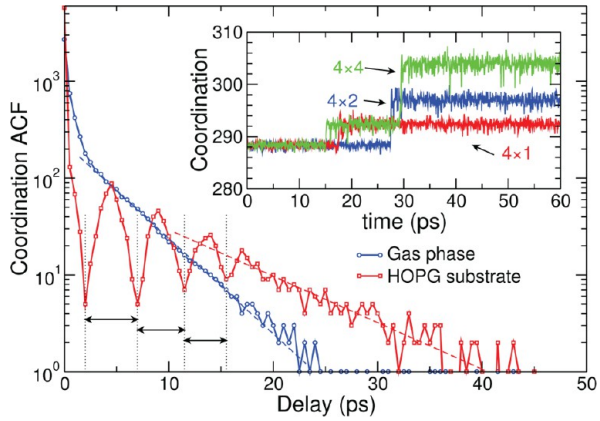

Figure 3. Time autocorrelation function $\langle C(t)\, C(t_0)\rangle$ of the coordination number $C(t)$ after the contact time t_0 between two $(MgO)_{32}$ cluster units, for coalescence in the gas phase and on the HOPG substrate. Some oscillations found in the latter case are highlighted by arrows. The inset shows the time variation of $C(t)$ for some typical trajectories on the HOPG substrate, leading to several products represented in Figure 1.

where we have represented the coordination number $C(t)$ as a function of time for three representative simulations, the results being averaged over 0.1 ps (100 time steps) to reduce the thermal noise. C is a suitable order parameter distinguishing the initial cubic structures (C = 144 × 2 = 288) from the compact 4 × 4 dimer (C = 288 + 16 = 304). While 4 × p products with p = 2 or 3 are formed directly, the 4 × 4 dimer may thus result from rearrangement of the 4 × 1 product. The kinetics of this isomerization process, whose relevance in oriented aggregation has been emphasized earlier by Spagnoli and co-workers,[36] can be addressed by monitoring the time autocorrelation function (ACF) $\langle C(t)\, C(t_0)\rangle$ at times $t > t_0$, where t_0 measures the contact time between the two monomers defined when their geometric distance becomes lower than 2.5 Å. The time variations of this ACF, as obtained from the selection of collisions in the gas phase or in presence of the substrate, are represented as the main plot in Figure 3. The ACT exhibits exponentially decaying variations over a characteristic time of 4.7 ps for free collisions, and 9.8 ps for collisions between deposited clusters. However, substrate-mediated collisions also display some periodic variations in $C(t)$ during the earliest 20 ps. Those variations are due to the oscillatory motion occurring around the 4 × 1 product, which is a shallow minimum along this soft normal mode. Once thermal excess energy overcomes the barrier, the systems interconverts into the more stable 4 × 4 product. Repeating the simulations for uncorrugated substrates essentially produces the same results, with comparably long oscillations (results not shown). Therefore, coalescence between two $(MgO)_{32}$ monomers largely proceeds by reorientation and rotational motion of the two cubes, the kinetic energy released by this mechanisms being dissipated into the substrate.

However, free collisions do not yield such oscillatory motion to the same extent. The reason behind this different behavior lies in the broader variety of dimers obtained just at contact, only a subset of them falling into the 4 × 1 product. Most structures produced at the contact time t_0 are very diverse and rearrange into one of the n × p dimers over a time scale that depends on its distance to this minimum, as well as on the available kinetic energy. This diversity of situations washes out the oscillatory pattern obtained when the contact clearly belongs to the 4 × 1 type.

Those results highlight the importance of the environment on the effective interactions between nanoclusters, besides facetting[36,48,49] and temperature[50] effects. They also confirm the role of kinetics and structural rearrangements on the coalescence products obtained over short time collisions, even for a particularly stable crystalline monomer. Taking now the nonmagic $(MgO)_{13}$ cluster as a building block, there are many more ways to assemble into corresponding dimers. The present potential predicts defective 3 × 3 × 3 cubes (with either oxygen

dx.doi.org/10.1021/jp410259b | J. Phys. Chem. C 2014, 118, 1306−1317

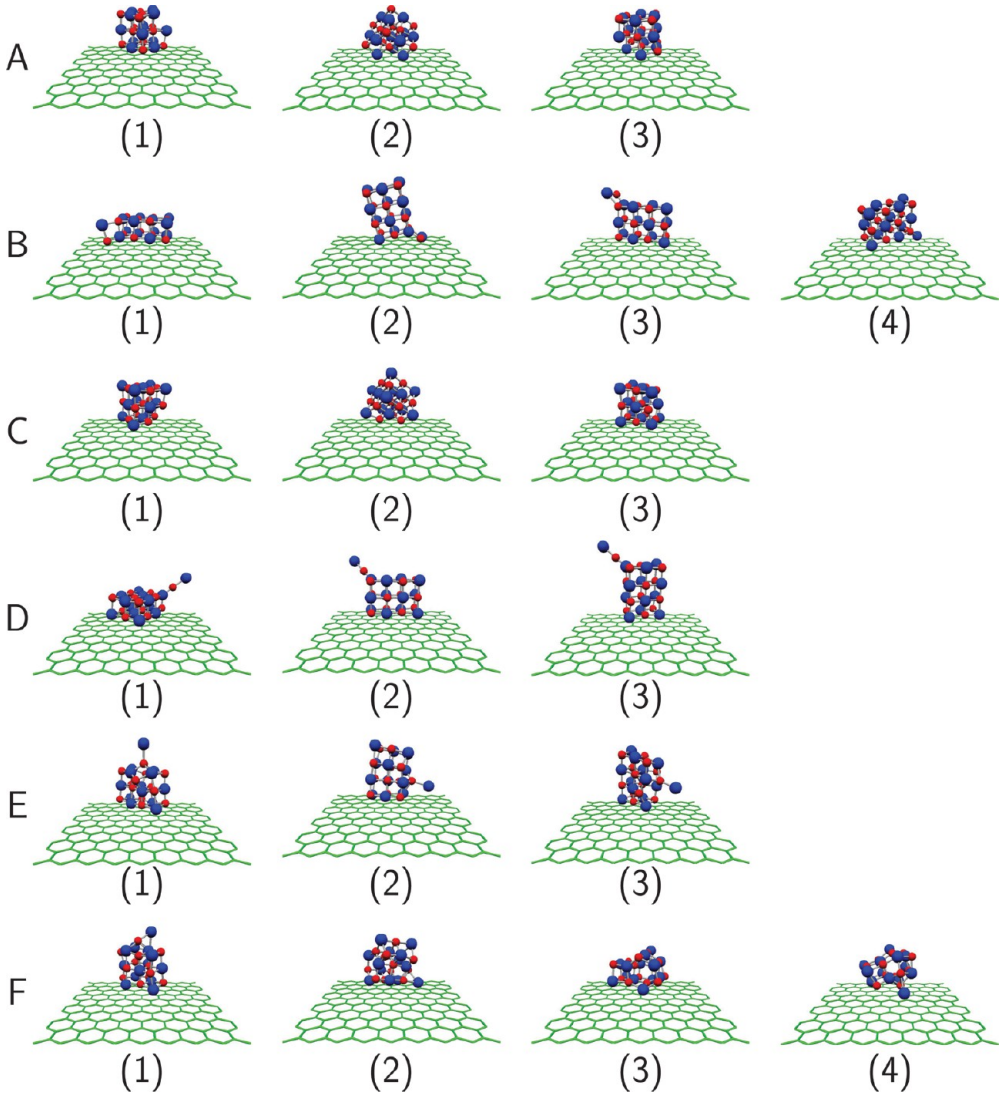

Figure 4. Coexisting forms M(m) of the $(MgO)_{13}$ cluster unit, alphabetically ordered (M = A–F) in the gas phase and differing in energy due to the contact interaction with the HOPG substrate (m index also referred to in Table 4).

or magnesium ions at the corners), but the hollow cage suggested from DFT calculations[27] is significantly higher in energy (we note in passing that conclusive experimental assignment has not been achieved yet for this cluster). Deposition on the graphite substrate produces additional isomers depending on the orientation and the area exposed to the surface. The degeneracy of the 6 lowest-energy isomers (A–F) obtained with the present potential is thus lifted, giving rise to 20 stable structures depicted in Figure 4 and denoted M(m) with M = A–F and m = 1–4 depending on M.

The energetic data for the isolated and deposited isomers of $(MgO)_{13}$ are given in Table 4, at 0 K but also at 300 K, after considering the entropy contribution in the harmonic free energies (with quantum oscillators). All cohesion energies are given relative to the global minima, for which the absolute values are tabulated. Only relative values are given for the free energies.

At 0 K, most of these 20 minima lie less than 0.5 eV above the most stable structure, which remains the 3 × 3 × 3 cube with an oxygen vacancy at a corner. However, the gas-phase ordering is somewhat scrambled due to the interaction with the substrate, an effect that is further magnified if we now consider the relative free energies at 300 K. The corresponding ordering is found to differ up to rank 18 with respect to the static ordering. More importantly, several deposited isomers are separated from the global free energy minimum by 0.1 eV or less, making them likely to be populated at thermal equilibrium.

The coalescence between $(MgO)_{13}$ monomers on graphite has been simulated using the same protocol as for $(MgO)_{32}$, with the only difference that the initial structures for both colliding monomers are randomly drawn from the list of 20 minima, given the 300 K statistical probability corresponding to the free energies also reported in Table 4. The multiple combinations of structures, together with the different sides exposed by these structures, lead to numerous possible products that are best sorted according to their binding energy after local optimization. The probability of forming a dimer with a specific binding energy is represented in Figure 5 as an histogram, as obtained from a set of 1000 successfully colliding trajectories. This distribution ranges over 0.15 eV and shows one main peak with additional smaller side peaks. Inspection of individual peaks often shows a variety of isomers, but the products are generally rather defective or partly hollow. Usually the deformations of individual clusters are minor and consist

dx.doi.org/10.1021/jp410259b | J. Phys. Chem. C 2014, 118, 1306–1317

Table 4. Energetic and Thermodynamical Properties of $(MgO)_{13}$ Isomers, Labeled as M(m) According to the Isolated Minimum (M = A−F) and the Different Ways (m) by Which the Minimum M Is in Contact with the HOPG Substrate[a]

	isomer	energy (0 K)	free energy (300 K)	probability (300 K)
A	isolated	7.05 eV/ion	0	1
	deposited (1)	7.10 eV/ion	0	0.75
	deposited (2)	+0.17 eV	+0.06 eV	0.07
	deposited (3)	+0.20 eV	+0.15 eV	0.02
B	isolated	+0.58 eV	+0.66 eV	0
	deposited (1)	+0.09 eV	+0.05 eV	0.11
	deposited (2)	+0.11 eV	+0.09 eV	0.02
	deposited (3)	+0.25 eV	+0.08 eV	0.03
	deposited (4)	+0.31 eV	+0.17 eV	0.00
C	isolated	+0.62 eV	+0.43 eV	0
	deposited (1)	+0.15 eV	+0.19 eV	0.00
	deposited (2)	+0.34 eV	+0.23 eV	0.00
	deposited (3)	+0.36 eV	+0.26 eV	0.00
D	isolated	+0.63 eV	+0.54 eV	0
	deposited (1)	+0.40 eV	+0.13 eV	0.00
	deposited (2)	+0.43 eV	+0.31 eV	0.00
	deposited (3)	+0.47 eV	+0.34 eV	0.00
E	isolated	+0.67 eV	+0.60 eV	0
	deposited (1)	+0.55 eV	+0.37 eV	0.00
	deposited (2)	+0.58 eV	+0.49 eV	0.00
	deposited (3)	+0.62 eV	+0.57 eV	0.00
	deposited (3)	+0.61 eV	+0.45 eV	0.00
F	isolated	+0.71 eV	+0.79 eV	0
	deposited (1)	+0.65 eV	+0.55 eV	0.00
	deposited (2)	+0.72 eV	+0.66 eV	0.00
	deposited (3)	+0.78 eV	+0.71 eV	0.00

[a]The absolute energy is given for the most stable isomers, the values for other minima being tabulated relative to the global minimum. The relative free energies at 300 K are based on the harmonic frequencies, and the equilibrium probabilities equivalent to those free energies are also given.

mostly of the displacement of the most flexible ions around vacancies or tails, when present. This notably occurs for the free-energy isomers B(1−4), D(1−3), E(1−3) and F(1−2) in Figure 4. The most probable product, although relatively compact, shows an uncomplete bond network at the contact between the two building blocks. Such dimers obtained by collisions usually keep the shape of the individual building blocks, with minor rearrangements at contact. The most stable dimers (higher cohesion energy) bear more resemblance to defective rocksalt structures, whereas less stable products typically result from mismatched orientations (see Figure 5). From those products, isomerizations toward the free-energy global minimum are expected to occur stepwise, over much longer time scales of microseconds.[51]

4. TOWARD LARGER SELF-ASSEMBLIES

Having characterized the structure and formation of MgO cluster dimers on the graphite substrate, we now extend our computational modeling to larger assemblies comprising many

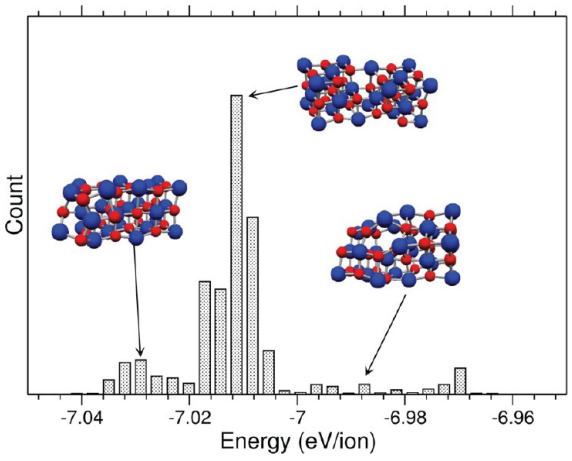

Figure 5. Probability distribution of the dimers produced from coalescence of two $(MgO)_{13}$ monomers on the HOPG substrate, as a function of their binding energy. Some dimers are depicted.

clusters. Due to the self-consistent determination of the charges at each time step, the fluctuating charges potential becomes too expensive. Although alternate schemes are available to alleviate such difficulties,[39,52] they still turned out to be rather cumbersome, limiting the possible simulation to a few tens of clusters with reasonable statistics. The simplified coarse-grained model with fixed charges proved sufficient to reproduce the statistics of dimers produced in the gas-phase collisions between two $(MgO)_{32}$ monomers. It was applied here to model the growth of the assembly, assuming a sequential process in which the assembly is locally relaxed between successive addition of monomers.

Figure 6a depicts a typical assembly of 200 $(MgO)_{32}$ clusters deposited sequentially on the HOPG substrate and coalescing

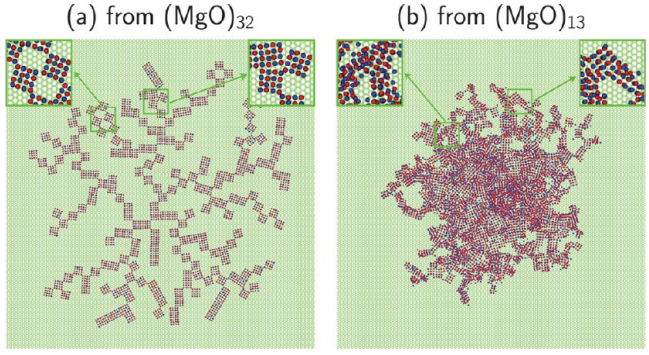

Figure 6. Typical assemblies produced by successive coalescence between $(MgO)_n$ cluster units on the HOPG substrate at T = 300 K. (a) $(MgO)_{32}$; (b) $(MgO)_{13}$. For each assembly, some specific regions are highlighted in the upper left and right corners.

by successive diffusion according to the model described previously. This assembly shows a highly ramified pattern, as has also been obtained on other surface-assembled metallic nanoparticles.[16,19] The mechanisms causing such a fractal-like pattern have been identified before[19] and consist essentially of diffusion-limited aggregation (DLA).[53] Although interactions between $(MgO)_{32}$ monomers are directional and anisotropic, the rocksalt structure preserved in the dimers conveys to the larger assembly but only locally, the organization between monomers being largely disordered in this ramified arrangement.

dx.doi.org/10.1021/jp410259b | J. Phys. Chem. C 2014, 118, 1306−1317

Oriented aggregation between clusters often occurs in this arrangement; however, many clusters do not accommodate with the crystallographic axes of the existing assembly. By looking more closely into the atomic details of the assembly, additional causes for this global disorder can be inferred. The high stability of the 4 × 1 dimer is reflected on the frequent motif where monomers are bound at edges, rather than faces. This is illustrated in the upper left corner of Figure 6a. The assembly of $(MgO)_{32}$ clusters also displays voids due to unfavorable positions of ions of the same sign. Frustration arises when a new monomer cannot accommodate the ionic bonds already present on the deformed assembly, and becomes trapped into noncrystalline positions. An example of these frustration-induced voids is depicted in Figure 6a in the upper right corner. As long as the incoming cluster is free to move on the 2D substrate, and without annealing, such defects should necessarily occur and prevent a clean aggregation over long distances.

Despite those defects, the assembly from $(MgO)_{32}$ clusters remains at least locally ordered. A rather different picture emerges if $(MgO)_{13}$ is used as the building block of the cluster assembly. In this case, successive building blocks are randomly selected from the thermal population of isomers at 300 K, and the resulting assembly is made of different minima. The assembly obtained from $(MgO)_{13}$, shown in Figure 6b, is clearly more dense and not as ramified as the assembly produced by coalescing $(MgO)_{32}$ cubic clusters. The structure of building blocks is mostly preserved in the assembly, but mostly in its outermost regions as depicted in the upper right corner of Figure 6b. However, as more minima coalesce on these outer regions, they usually react through the defects to produce locally disordered arrangements, as highlighted in the upper left corner of Figure 6b.

Besides visual inspection, a more robust structural analysis is presented in Figure 7 with the pair distribution functions $g(r)$ between magnesium and oxygen ions, and the distribution $p(z)$ of distances of Mg ions to the HOPG surface, both quantities being obtained from 10 independent realizations of $[(MgO)_{32}]_{400}$ assemblies. The assembly created from cubic $(MgO)_{32}$ monomers exhibits narrow peaks in those two distributions, confirming the high degree of local order consistent with the natural rocksalt alignment preserved upon dimer formation, also observed in MD simulations of interacting PbSe nanocrystals.[49]

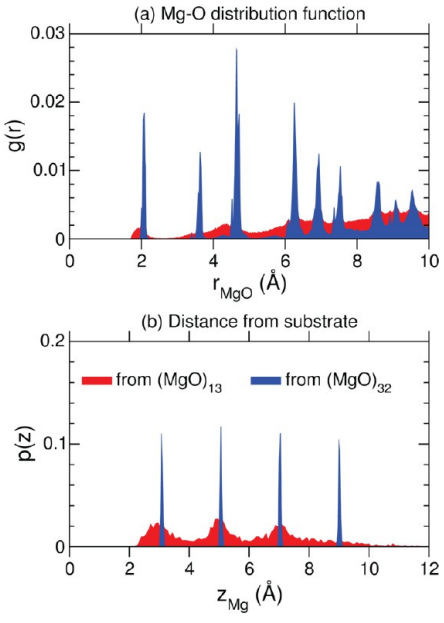

Figure 7. Geometric properties of the assemblies obtained by successive coalescence of 400 $(MgO)_{32}$ or $(MgO)_{13}$ units on the HOPG substrate. (a) Mg−O pair distribution function; (b) distance of magnesium ions to the substrate.

In particular, the four peaks in $p(z)$ show that all cubes in the $[(MgO)_{32}]_{400}$ assembly remain parallel to the substrate, the assembly itself being perfectly bidimensional. In contrast, the $[(MgO)_{13}]_{400}$ assembly shows much broader peaks in both distributions, indicating a significant extent of local disorder. The spreading of the two structural parameters and the extension of the height distribution toward higher z values slightly beyond 10 Å indicate that this assembly has a more pronounced 3D shape, and a globally amorphous character. These major differences arise due to the lesser stability of the $(MgO)_{13}$ cluster, which in most of its coexisting isomers significantly deviates from the perfect crystallinity of $(MgO)_{32}$. The diversity of dimers produced from coalescing two such clusters (see Figure 5) largely explains this amorphous structure, from the major atomic rearrangement undergone by the approaching clusters upon contact. Such rearrangements are particularly clear on the occasional migration of ions to higher z that occurs by merging defects of different types (vacancies with tails), thereby increasing the overall cohesion energy.

We end this section by further comparing our results to experimental measurements on the self-assembly of $(PbS)_{32}$ clusters. At low coverage, earlier work[37] has shown that those building blocks tend to grow by oriented aggregation. Additional experiments have been performed for the same systems but at high coverage, and a typical snapshot by scanning tunneling microscopy is represented in Figure 8. The

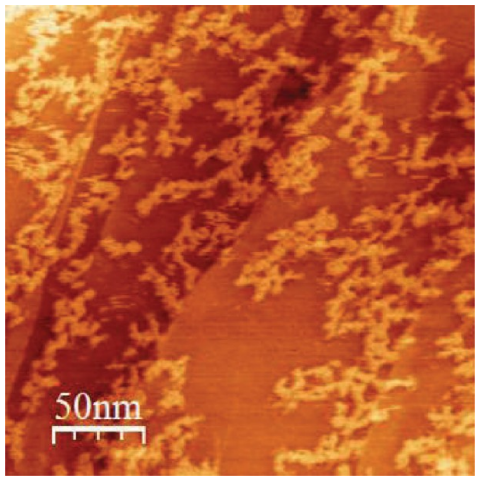

Figure 8. Scanning tunneling microscope (STM) image of an assembly of $(PbS)_{32}$ clusters deposited on HOPG, at high coverage.

pattern is clearly fractal-like, in agreement with our simulation results on $(MgO)_{32}$ clusters. This comparison confirms that, besides chemical differences between MgO and PbS, the time scales associated with reorientation of the clusters as they approach the existing assembly are crucial for the growth of the assembly. At low coverage, the clusters have more time to relax on the substrate, and rearrange to form regular assemblies. In

dx.doi.org/10.1021/jp410259b | J. Phys. Chem. C 2014, 118, 1306−1317

contrast, a high coverage is equivalent to a faster sequential addition of clusters, as presently simulated, which favors geometric frustration, voids and leads to ramification of the assembly.

5. CONCLUDING REMARKS

Exploiting the specific properties of clusters into self-assembled materials requires those clusters to be either particularly stable against coalescence and preserve their identity upon assembling or, if orientated aggregation is sought, to grow along well-defined directions. Bare MgO clusters exhibit essentially ionic bonds, and form the rocksalt motif already at the magic size of 32 pairs of ions, other clusters forming defective or more open structures. In the present work, we have identified the dominant pathways taking place in the early steps of MgO clusters coalescence in vacuum and in the more realistic situation of deposition of many clusters on the chemically inert graphite substrate. Of particular interest, the role of the building block has been addressed here by performing explicit simulations at the atomistic level. By comparing the way $(MgO)_n$ clusters interact with each other depending on their intrinsic stability, we have highlighted the important roles of the substrate and the possible coexisting isomers on the diversity in the cluster dimers produced under mild thermal collisions.

The substrate acts as a major constraint on the cluster−cluster interaction, especially since the MgO−graphite bond is rather weak and mostly attracts the cluster to maximize the contact area, corrugation being a minor correction to binding. Due to the cluster−substrate interaction, $(MgO)_{13}$ clusters display a richer diversity of isomers relative to the gas phase, differing mostly in the contact area with the substrate. Coalescence between different $(MgO)_{13}$ monomers statistically produces largely noncrystalline dimers, which translates into larger assemblies with a high amorphous character. In contrast, the rocksalt order in the $(MgO)_{32}$ monomer is locally preserved in the assembly, which due to diffusion-limited aggregation mechanisms grows along a ramified pattern.

The present MgO clusters necessarily coalesce in absence of chemical protection, preventing the formation of periodic assemblies of intact individual building blocks. In particular, honeycomb corrugation of the graphite substrate appears clearly unsufficient to trap clusters, the ionic bonds dominating the interactions. The growth of larger assemblies from bare $(MgO)_n$ clusters is thus essentially driven by geometric considerations arising from the absence (n = 32) or presence (n = 13) of structural defects in the monomeric units. However, even when the building blocks are crystalline, orientated aggregation along privileged directions is difficult due to the time needed for reorientation and the ramification of the arrangement along noncrystalline directions caused by geometric frustration and voids.

Our simulation results are consistent with earlier measurements on the chemically and structurally similar PbS clusters deposited on graphite at low coverage,[37] which tend to grow by oriented aggregation. At high coverage, experiments reveal fractal-like patterns similar to the predictions of our model. It would thus seem natural to extend the present work to treat directly PbS clusters, especially considering that PbS nanocrystals are known to be prone to oriented attachment.[7] However this would require parametrization of a model potential, a task demanding some dedicated efforts, possibly at the ab initio level. In addition, experimental measurements on other metal oxide nanoparticles[5,54] should also be able to assess some our predictions. Alternatively to changing the clusters, different substrates could be studied as well. For instance, folded graphene sheets[56] or carbon nanotubes[55] could present strong curvature effects[55,57] that could be addressed computationally using effective coarse-grained potentials.[58] Another interesting research avenue could focus on more dynamical or kinetic issues. Preliminary MD simulations of individual $(MgO)_{32}$ clusters indicate some substantial mobility at 300 K (diffusion constant $D \sim 0.7$ Å^2/ps), but it is unclear how the diffusion changes with cluster size, the isomer, and to which extent it impacts the larger assemblies, be they fractal or amorphous.

As far as modeling is concerned, and besides the development of a dedicated potential for PbS, it would be useful to go beyond the rigid substrate approximation, although a complete model for describing MgO clusters on flexible graphite is lacking. Combining the present potential with an accurate carbon model such as the recent LCBOPII potential of Los and co-workers[59] could be one way to tackle this issue. Incidentally, such a model would also provide a suitable computational framework to study the soft-landing process itself, and get insight into the time scales for reorientation and thermalization during assembly. Conversely, further levels of coarse-graining could be attempted along the lines of our fully rigid model, for instance by developing a simplified model for the interaction between MgO nanocrystals based on the more detailed polarizable potential. Although it would work best for the symmetric $(MgO)_{32}$ cluster than for the isomerizing $(MgO)_{13}$ case, such an approach would pave the way to larger-scale simulations, along the lines of lattice-based models,[60] and even lead to some estimate of the fractal dimension of the resulting assemblies.

AUTHOR INFORMATION

Corresponding Author

*E-mail:florent.calvo@univ-lyon1.fr.

Notes

The authors declare no competing financial interest.

ACKNOWLEDGMENTS

F.C. would like to thank the Pôle Scientifique de Modélisation Numérique (PSMN) in Lyon, France, for generous allocations of computer time. This material is based in part on work supported by the AFOSR under Grant Number FA9550-11-1-0068 (K.B.).

REFERENCES

(1) Perez, A.; Melinon, P.; Dupuis, V.; Jensen, P.; Prevel, B.; Tuaillon, J.; Bardotti, L.; Martet, C.; Treilleux, M.; Broyer, M.; Pellarin, M.; Vialle, J.-L.; Palpant, B.; Lerme, J. Cluster assembled materials: A novel class of nanostructured solids with original structures and properties. *J. Phys. D: Appl. Phys.* **1997**, *30*, 709−721.

(2) Waychunas, G. A. Structure, aggregation and characterization of nanoparticles. *Rev. Mineral. Geochem.* **2001**, *44*, 105−166.

(3) Claridge, S. A.; Castleman, A. W., Jr.; Khanna, S. N.; Murray, C. B.; Sen, A.; Weiss, P. S. Cluster-assembled materials. *ACS Nano* **2009**, *3*, 244−255.

(4) Penn, R. L.; Banfield, J. F. Imperfect oriented attachment: Dislocation generation in defect-free nanocrystals. *Science* **1998**, *281*, 969−971.

(5) Pacholski, C.; Kornoswki, A.; Weller, H. Self-assembly of ZnO: From nanodots to nanorods. *Angew. Chem., Int. Ed.* **2002**, *41*, 1188−1191.

(6) Cho, K.-S.; Talapin, D. V.; Gaschler, W.; Murray, C. B. Designing PbSe nanowires and nanorings through oriented attachment of nanoparticles. *J. Am. Chem. Soc.* **2005**, *127*, 7140−7147.
(7) Schliehe, C.; Juarez, B. H.; Pelletier, M.; Jander, S.; Greshnykh, D.; Nagel, M.; Meyer, A.; Foerster, S.; Kornowski, A.; Klinke, C.; Weller, H. Ultrathin PbS sheets by two-dimensional oriented attachment. *Science* **2010**, *329*, 550−553.
(8) Li, D.; Nielsen, M. H.; Lee, J. R. I.; Frandsen, C.; Banfield, J. F.; De Yoreo, J. J. Direction-specific interactions control crystal growth by oriented attachment. *Science* **2012**, *336*, 1014−1018.
(9) N'Diaye, A. T.; Bleikamp, S.; Feibelman, P. J.; Michely, T. Two-dimensional Ir cluster lattice on a graphene moire on Ir(111). *Phys. Rev. Lett.* **2006**, *97*, 215501.
(10) Brihuega, I.; Michaelis, C. H.; Zhang, J.; Bose, S.; Sessi, V.; Jonolka, J.; Schneider, M. A.; Enders, A.; Kern, K. Electronic decoupling and templating of Co nanocluster arrays on the boron nitride nanomesh. *Surf. Sci.* **2008**, *602*, L95−L99.
(11) Collier, C. P.; Vossmeyer, T.; Heath, J. R. Nanocrystal superlattices. *Annu. Rev. Phys. Chem.* **1998**, *49*, 371−404.
(12) Murray, C. B.; Kagan, C. R.; Bawendi, M. G. Synthesis and characterization of monodisperse nanocrystals and close-packed nanocrystal assemblies. *Annu. Rev. Mater. Sci.* **2000**, *30*, 545−610.
(13) Manna, L.; Milliron, D. J.; Meisel, A.; Scher, E. C.; Alivisatos, A. P. Controlled growth of tetrapod-branched inorganic nanocrystals. *Nat. Mater.* **2003**, *2*, 382−385.
(14) Burda, C.; Chen, X. B.; Narayanan, R.; El-Sayed, M. A. Chemistry and properties of nanocrystals of different shapes. *Chem. Rev.* **2005**, *105*, 1025−1102.
(15) Tao, A. R.; Habas, S.; Yang, P. D. Shape control of colloidal metal nanocrystals. *Small* **2008**, *4*, 310−325.
(16) Yoon, B.; Akulin, V. M.; Cahuzac, P.; Carlier, F.; de Frutos, M.; Masson, A.; Mory, C.; Colliex, C.; Bréchignac, C. Morphology control of the supported islands grown from soft-landed clusters. *Surf. Sci.* **1999**, *443*, 76−88.
(17) Zheng, W.-J.; Thomas, O. C.; Lippa, T. P.; Xu, S.-J.; Bowen, K. H., Jr. The ionic KAl_{13} molecule: A stepping stone to cluster-assembled materials. *J. Chem. Phys.* **2006**, *124*, 144304.
(18) Bromann, K.; Brune, H.; Félix, C.; Harbich, W.; Monot, R.; Buttet, J.; Kern, K. Hard and soft landing of mass selected Ag clusters on Pt(111). *Surf. Sci.* **1997**, *377−379*, 1051−1055.
(19) Jensen, P. Growth of nanostructures by cluster deposition: Experiments and simple models. *Rev. Mod. Phys.* **1999**, *71*, 1965−1735.
(20) Lalatonne, Y.; Richardi, J.; Pileni, M.-P. Van der Waals versus dipolar forces controlling mesoscopic organizations of magnetic nanocrystals. *Nat. Mater.* **2004**, *3*, 121−125.
(21) Millett, P. C.; Wang, Y. U. Diffuse interface field approach to modeling and simulation of self-assembly of charged colloidal particles of various shapes and sizes. *Acta Mater.* **2009**, *57*, 3101−3109.
(22) Lutsko, J. F.; Basios, V.; Nicolis, G.; Caremans, T. P.; Aerts, A.; Martens, J. A.; Kischhock, C. E. A.; van Erp, T. S. Kinetics of intermediate-mediated self-assembly in nanosized materials: A generic model. *J. Chem. Phys.* **2010**, *132*, 164701.
(23) Whitelam, S. Nonclassical assembly pathways of anisotropic particles. *J. Chem. Phys.* **2010**, *132*, 194901.
(24) Castleman, A. W., Jr.; Khanna, S. N. Clusters, superatoms, and building blocks of new materials. *J. Phys. Chem. C* **2009**, *113*, 2664−2675.
(25) Koparde, V. N.; Cummings, P. T. Molecular dynamics simulation of titanium dioxide nanoparticle sintering. *J. Phys. Chem. B* **2005**, *109*, 24280−24287.
(26) Ziemann, P. J.; Castleman, A. W. Stabilities and structures of gas-phase MgO clusters. *J. Chem. Phys.* **1991**, *94*, 718−728.
(27) Haertelt, M.; Fielicke, A.; Meijer, G.; Kwapien, K.; Sierka, M.; Sauer, J. Structure determination of neutral MgO clusters-hexagonal nanotubes and cages. *Phys. Chem. Chem. Phys.* **2012**, *14*, 2849−2856.
(28) Köhler, T. M.; Gail, H. P.; Sedlmayr, E. MgO dust nucleation in M-stars: Calculation of cluster properties and nucleation rates. *Astron. Astrophys.* **1997**, *320*, 553−567.
(29) de la Puente, E.; Aguado, A.; Ayuela, A.; Lopez, J. M. Structural and electronic properties of small neutral $(MgO)_n$ clusters. *Phys. Rev. B* **1997**, *56*, 7607−7614.
(30) Wilson, M. Stability of small MgO nanotube clusters: Predictions of a transferable ionic potential model. *J. Phys. Chem. B* **1997**, *101*, 4917−4924.
(31) Roberts, C.; Johnston, R. L. Investigation of the structures of MgO clusters using a genetic algorithm. *Phys. Chem. Chem. Phys.* **2001**, *3*, 5024−5034.
(32) Calvo, F. Crossover between ionic-covalent bonding and pure ionic bonding in magnesium oxide clusters. *Phys. Rev. B* **2003**, *67*, 161403(R).
(33) Bhatt, J. S.; Ford, I. J. Investigation of MgO as a candidate for the primary nucleating dust species around M stars. *Mon. Not. R. Astron. Soc.* **2007**, *382*, 291−298.
(34) Carrasco, J.; Illas, F.; Bromley, S. T. Ultralow-density nanocage-based metal-oxide polymorphs. *Phys. Rev. Lett.* **2007**, *99*, 235502.
(35) Dong, R. B.; Chen, X. S.; Wang, X. F.; Lu, W. Structural transition of hexagonal tube to rocksalt for $(MgO)_{3n}$, $2 \leq n \leq 10$. *J. Chem. Phys.* **2008**, *129*, 044705.
(36) Spagnoli, D.; Banfield, J. F.; Parker, S. C. Free energy change of aggregation of nanoparticles. *J. Phys. Chem. C* **2008**, *112*, 14731−14736.
(37) Kiran, B.; Kandalam, A. K.; Rallabandi, R.; Koirala, P.; Li, X.; Tang, X.; Wang, Y.; Fairbrother, H.; Ganteför, G.; Bowen, K. H. $(PbS)_{32}$: A baby crystal. *J. Chem. Phys.* **2012**, *136*, 024317.
(38) Rappé, A. K.; Goddard, W. A., III. Charge equilibration for molecular dynamics simulations. *J. Phys. Chem.* **1991**, *95*, 3358−3363.
(39) Rick, S. W.; Stuart, S. J.; Berne, B. J. Dynamical fluctuating charge force fields - Application to liquid water. *J. Chem. Phys.* **1994**, *101*, 6141−6156.
(40) Ohno, K. Some remarks on the Pariser-Parr-Pople method. *Theor. Chim. Acta* **1964**, *2*, 219−227.
(41) Jorgensen, W. L.; Maxwell, D. S.; Tirado-Rives, J. Development and testing of the OPLS all-atom force field on conformational energetics and properties of organic liquids. *J. Am. Chem. Soc.* **1996**, *118*, 11225−11236.
(42) Steele, W. A. The physical interaction of gases with crystalline solids. I. Gas-solid energies and properties of isolated adsorbed atoms. *Surf. Sci.* **1973**, *36*, 317−352.
(43) González, B. S.; Hernández-Rojas, J.; Bretón, J.; Gomez Llorente, J. M. Global potential energy minima of $(H_2O)_n$ clusters on graphite. *J. Phys. Chem. C* **2007**, *111*, 14862−14869.
(44) Böttcher, A.; Weiss, P.; Bihlmeier, A.; Kappes, M. M. C_{58} on HOPG: soft-landing adsorption and thermal desorption. *Phys. Chem. Chem. Phys.* **2004**, *6*, 5213−5217.
(45) Hamaker, H. C. The London-van der Waals attraction between spherical particles. *Physica* **1937**, *10*, 1058−1072.
(46) Korgel, B. A.; Fitzmaurice, D. Self-assembly of silver nanocrystals into two-dimensional nanowire arrays. *Adv. Mater.* **1998**, *10*, 661−665.
(47) Theissmann, R.; Fendrich, M.; Zinetullin, R.; Guenther, G.; Schierning, G.; Wolf, D. E. Crystallographic reorientation and nanoparticle coalescence. *Phys. Rev. B* **2008**, *78*, 205413.
(48) Schapotschnikow, P.; Pool, R.; Vlugt, T. J. H. Molecular simulations of interacting nanocrystals. *Nano Lett.* **2008**, *8*, 2930−2934.
(49) Schapotschnikow, P.; van Huis, M. A.; Zandbergen, H. W.; Vanmaekelbergh, D.; Vlugt, T. J. H. Morphological transformations and fusion of PbSe nanocrystals studied using atomistic simulations. *Nano Lett.* **2010**, *10*, 3966−3971.
(50) Calvo, F.; Spiegelmann, F. Thermodynamical study of the interaction between clusters. *Phys. Rev. B* **1996**, *54*, 10949−10958.
(51) Doye, J. P. K.; Wales, D. J. The dynamics of structural transitions in sodium chloride clusters. *J. Chem. Phys.* **1999**, *111*, 11070−11079.
(52) Calvo, F. Role of charge localization on the Coulomb fragmentation of large metal clusters: A model study. *Phys. Rev. A* **2006**, *74*, 043202.

(53) Witten, T. A.; Sander, L. M. Diffusion-limited aggregation, a kinetic critical phenomenon. *Phys. Rev. Lett.* **1981**, *47*, 1400−1403.
(54) Wepasnick, K. A.; Li, X.; Mangler, T.; Noessner, S.; Wolke, C.; Grossmann, M.; Ganteför, G.; Fairbrother, D. H.; Bowen, K. H. Surface morphologies of size-selected $Mo_{100\pm2.5}$ and $(MoO_3)_{67\pm1.5}$ clusters soft-landed onto HOPG. *J. Phys. Chem. C* **2011**, *115*, 12299−12307.
(55) Shu, D. J.; Gong, X. G. Curvature effect on surface diffusion: The nanotube. *J. Chem. Phys.* **2001**, *114*, 10922−10926.
(56) Kemper, A. F.; Cheng, H.-P.; Kébali, N.; Benrezzak, S.; Schmidt, M.; Masson, A.; Bréchignac, C. Curvature effect on the interaction between folded graphitic surface and silver clusters. *Phys. Rev. B* **2009**, *79*, 193403.
(57) Morrow, B. H.; Striolo, A. Platinum nanoparticles on carbonaceous materials: the effect of support geometry. *Nanotechnology* **2008**, *19*, 195711.
(58) Bretón, J.; González-Platas, J.; Girardet, C. Endohedral adsorption in graphitic nanotubules. *J. Chem. Phys.* **1994**, *101*, 3334−3340.
(59) Los, J. H.; Ghiringhelli, L.; Meijer, E.; Fasolino, A. Improved long-range reactive bond-order potential for carbon. I. Construction. *Phys. Rev. B* **2005**, *72*, 214102.
(60) Kim, H.; Schatz, G. C.; Jang, J. Simplistic model for the dendritic growth of a monolayer in dip pen nanolithography. *J. Phys. Chem. C* **2010**, *114*, 1922−1927.